Article ID: 1000-324X(2021)06-0665-08 **DOI:** 10.15541/jim20200356

CuS Nanosheet Decorated Bi_5O_7I Composite for the Enhanced Photocatalytic Reduction Activity of Aqueous Cr(VI)

CAI Miao, CHEN Zihang, ZENG Shi, DU Jianghui, XIONG Juan

(Hubei Key Laboratory of Ferro & Piezoelectric Materials and Devices, Faculty of Physics & Electronic Sciences, Hubei University, Wuhan 430062, China)

Abstract: Photocatalytic approach has been extensively explored to remove toxic Cr(VI) in wastewater owing to its high efficient, safe and low cost features. Fabricating semiconductor composite is supposed to be an effective approach to improve the poor photocatalytic activity of single component. In this work, we prepared CuS nanosheets decorated Bi_5O_7I composites by a simple hydrothermal method, and characterized and evaluated its photoatalytic reduction activity of Cr(VI) under the visible-light irradiation. Compared to pure Bi_5O_7I microrods and CuS nanoparticles, the as-prepared CuS/Bi_5O_7I composites exhibits more efficient photocatalytic reduction of aqueous Cr(VI). The reaction rate constant of 15wt% CuS/Bi_5O_7I catalyst was 20 times and 4.3 times of that of pristine Bi_5O_7I and CuS, respectively. BET, photoluminescence and EIS spectra measurement demonstrate that the improved photocatalytic activity may be attributed to their higher surface areas, broader light absorption region, improved separation, and transfer efficiency of photo-induced electron-hole pairs. Moreover, a possible photocatalytic mechanism of CuS/Bi_5O_7I catalyst is also proposed.

Key words: CuS/Bi_5O_7I composite photocatalyst; visible-light photocatalyst; photocatalytic reduction of Cr(VI)

The industrial production processes such as metal smelting, chemical industries, production of pigment, medicine and paper have given rise to heavy metal pollution which are harmful to human beings and other creatures in nature. Among the toxic heavy metal pollutants, the threaten to human being and ecological systems caused by hexavalent chromium (Cr(VI)) has attracted more and more attention since Cr(VI) has high solubility in aqueous solution, substantiated toxicity and potential carcinogenicity. Therefore, it is highly necessary to solve the Cr(VI) presence in wastewater[1-2]. Since the conventional approaches bring out the problems such as secondary pollution, onerous procedures and high energy consumption, the reduction of Cr(VI) to non-toxic Cr(III) which can be realized by semiconductor has attracted increasing attention with the advantages of low cost, environmental safety and high efficient utilization of solar energy[3-4]. Semiconductor photocatalytic method for the reduction of Cr(VI) to Cr(III) is ascribed to electron-hole pairs generated by energetic photons which lead to the photo redox process[5]. TiO_2 photocatalyst or TiO_2 based composites have received great attention because of high photocatalytic activity, favorable chemical stability and low-cost. However, its low photo-responsivity in the visible light hinders its practical utilization efficiency. Therefore, a large number of visible light response photocatalysts is designed and synthesized to improve the photocatalytic efficiency[6-7].

Among various photocatalysts, Bi-compounds based photocatalysts, such as Bi_2O_3, $BiVO_4$, Bi_2MoO_6, BiOX (X=Cl, Br, I) and $Bi_2O_2CO_3$ have been extensively reported with satisfactory photocatalytic performance for the degradation of organic pollutants and removal of Cr(VI) reduction[8-10]. As a member of bismuth family, Bi_5O_7I is currently discovered as visible-light-driven semiconductor with its optical band gap of about 2.8 eV. The characteristic layered crystal structure of Bi_5O_7I from the $[Bi_2O_2]^{2+}$ and double I layers could induce an internal static electric field which is perpendicular to each layer and subsequently beneficial for the separation of photo-generated carriers[11]. However, Bi_5O_7I suffered from the insufficient light absorption and fast recombination of electron-hole pairs which considerably restricted its

Received date: 2020-06-29; **Revised date:** 2020-08-13; **Published online:** 2020-10-23
Foundation item: National Natural Science Foundation of China (51972102)
Biography: CAI Miao(1996–), male, Master candidate. E-mail: zhangsan@mail.sic.ac.cn
蔡 苗(1996–), 男, 硕士研究生. E-mail: zhangsan@mail.sic.ac.cn
Corresponding author: XIONG Juan, associated professor. E-mail: juanxiong@hubu.edu.cn
熊 娟, 副教授. E-mail: juanxiong@hubu.edu.cn

extended practical applications in photocatalysis[12-13]. For practical application, many efforts have been devoted for improving photocatalytic property of Bi_5O_7I, containing designing metal-semiconductor composites, constructing semiconductor composites with proper band gap semiconductors or high specific surface area, such as g-C_3N_4/Bi_5O_7I, Ag_2O/Bi_5O_7I, AgI/Bi_5O_7I[14-16].

In addition, CuS, as a p-type photocatalyst with narrow band gap exhibits broad absorption spectra in the range from ultraviolet (UV) to near-infrared (NIR) region, has been extensively used as an efficient photocatalyst. For example, Lai, *et al.* [17] reported that CuS decorated $BiVO_4$ to enhance its photocatalytic property in ciprofloxacin degradation. Naghizadeh, *et al.* [18] reported that the $CoFe_2O_4$@CuS nanocomposite shows enhanced photocatalytic degradation of penicillin G antibiotic. Ghim, *et al.* [19] prepared $ZnMoS_4$/CuS p-n heterojunctions which exhibited efficient photocatalytic hydrogen generation. These results indicate that CuS could be a favorable co-catalyst for Bi_5O_7I photocatalyst. Yet there are little reports on the fabrication and photocatalytic reduction activity of Cr(VI) under visible light of CuS/Bi_5O_7I composite.

In this work, novel CuS/Bi_5O_7I composite was fabricated by a facile hydrothermal method. Bi_5O_7I microrods were decorated by CuS nanosheets, which was in favor of convenient and effective regulation of Bi_5O_7I-based composite's photocatalytic properties. The Cr(VI) aqueous solution is employed as the target degradation contamination to evaluate the photocatalytic performance of CuS/Bi_5O_7I. The photocatalytic experiments results manifested the improved photocatalytic reduction efficiency of CuS/Bi_5O_7I composites for aqueous Cr(VI) under visible light irradiation. Moreover, the possible mechanism of photocatalytic reduction of Cr(VI) by CuS/Bi_5O_7I composites was also explored.

1 Experimental

1.1 Synthesis of Bi_5O_7I microrods

Briefly, $Bi(NO_3)\cdot 5H_2O$ (4.85 g) was dissolved in deionized water (200 mL), ultrasonically dispersed for 30 min and kept stirring for 60 min and then 5 mL of acetic acid was added to obtain suspension A.

KI (1.66 g) was dissolved in deionized water (10 mL) to obtain homogeneous solution which was added to the suspension A dropwise and kept magnetic stirring for 30 min to obtain a black suspension B. After that, 4 mL ammonia water was added dropwise to suspension C until the brick red precipitation appeared. After magnetic stirring at 85 ℃ for 60 min, the BiOI red precipitate was obtained by centrifugation, and fully dried at 70 ℃. The BiOI red powder was then ultrasonically dispersed in a mixture solvent of ethanol and deionized water (25 mL/25 mL) for 30 min to obtain a suspension. Next, NaOH solution (25 mL 0.2 mmol/L) was added to the above suspension with vigorous stirring at 70 ℃ for 60 min. Finally, the white Bi_5O_7I sample was washed by deionized water and ethanol for several times and dried at 70 ℃ overnight.

1.2 Synthesis of CuS/Bi_5O_7I

CuS decorated Bi_5O_7I with different amounts of CuS was prepared as following: $CuSO_4\cdot 5H_2O$, thiourea and trisodium citrate dihydrate was dissolved in deionized water (30 mL). After stirring for 20 min, Bi_5O_7I powder were ultrasonically dispersed in the above solution for 30 min. The suspension was then transferred into a 50 mL Teflon-lined stainless autoclave and reacted at 160 ℃ for 10 h. Finally, the CuS/Bi_5O_7I composite was collected and washed by deionized water, and then dried at 60 ℃ for 10 h. CuS/Bi_5O_7I composites were denoted as CB-*x*, where *x* is the mass percentage (wt%) of CuS, and named as CB-10, CB-15 and CB-20, respectively. The fabrication process of CuS/Bi_5O_7I composites was presented in Scheme 1. By contrast, pure CuS were also prepared by the procedure described above without the addition of Bi_5O_7I.

1.3 Characterizations

The phase structure of the samples was determined by the Bruker D8 Advance powder X-ray diffractometer with Cu-Kα irradiation (λ=0.154056 nm). The morphologies and microstructural properties were obtained by field emission scanning electron microscope (FESEM, JSM-7100F, JEOL) and high-resolution transmission electron microscope (HRTEM, JEM 2010F). UV-Vis diffuse reflectance spectra were carried out on a UV-Vis spectrophotometer (UV-3600, Shimadzu) with an integrating sphere attachment. QDS-MP-30 volumetric gas adsorption instrument (Quantachrome, USA) was employed to measure the Brunauer-Emmett-Teller (BET) surface area. X-ray photoelectron spectroscopy (XPS) on an ESCALAB 250 xi apparatus was conducted to reveal the elemental composition and surface states of CuS/Bi_5O_7I composite. The photoluminescence (PL) spectra were determined by a fluorescence spectrophotometer (PerkinElmer, LS-55) at room temperature. A Zahner CIMPS electrochemical workstation (Germany) was employed to perform the electrochemical impedance spectra (EIS) measurement in a three-electrode system with Pt wire and Ag/AgCl electrode as the counter and reference electrodes, respectively. Pure Bi_5O_7I, CuS or CB-15 composites spin-coated ITO with the size of 1 cm×1 cm was used as working electrode. The measurement was carried out in 0.2 mol/L Na_2SO_4 aqueous solution.

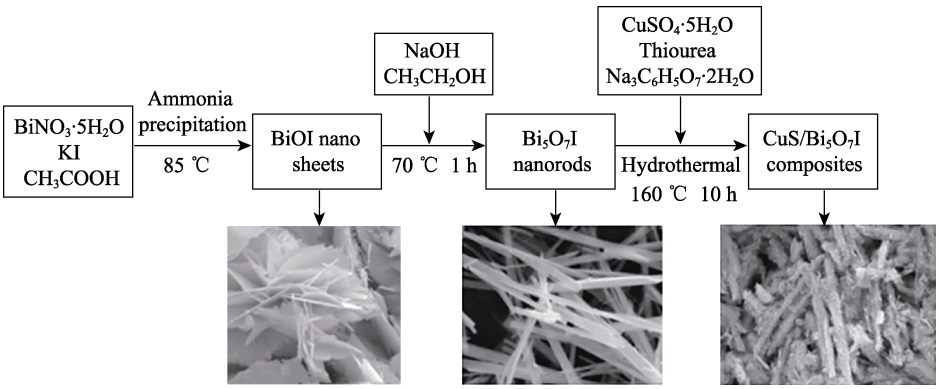

Scheme 1 Preparation process diagram of CuS/Bi_5O_7I composites

1.4 Photocatalytic activity

The photocatalytic properties of the as-synthesized photocatalysts were accessed for the reduction of Cr(VI) to Cr(III) and performed in aqueous solution with concentration of 10 mg/L. The pH of the mixture solution should be controlled at about 3 with H_2SO_4 solutions. In the photocatalytic activity evaluation experiment, 100 mg sample was added to 150 mL $K_2Cr_2O_7$ aqueous solutions and kept magnetic stirring for 30 min to reach adsorption/desorption equilibrium. Then, the illumination from a 300 W Xe lamp equipped with 420 nm cutoff filter to make sure the photocatalytic reduction reaction take place under the visible-light irradiation. During the irradiation, 3 mL suspensions were sucked out at given time intervals. After removing the solid photocatalyst by centrifuging and filtration, the concentration of Cr(VI) in the filtrate was measured according to the diphenylcarbazide colorimetric method determined by Shimadzu UV-3600 spectrophotometer. The photocatalytic reduction activity was evaluated by the time-depending C/C_0, where C is the remained Cr(VI) concentration and C_0 is the initial Cr(VI) concentration.

2 Results and discussion

X-ray diffraction patterns of as-prepared Bi_5O_7I, CuS and CuS/Bi_5O_7I composites are presented in Fig. 1. It can be seen that XRD peaks at 2θ=27.9°, 28.9°, 30.9°, 33°, 45.9°, 53.6° and 56.1° correspond to (312), (113), (004), (204), (604), (224), (316) and (912) crystal planes of orthorhombic Bi_5O_7I, respectively. The synthesized Bi_5O_7I is well-crystallized, and all of the peaks are indexed to the standard card (JCPDS 40-0548) without other impurity phase[15]. The diffractions for pure CuS almost exactly match the standard cards JCPDS 06-0464[17]. For CuS/Bi_5O_7I composites, no characteristic diffraction peaks of CuS were detected when the content of CuS is lower than 15wt%. However, the character peak of CuS at 2θ=31.8° could be observed in the CB-20 composite.

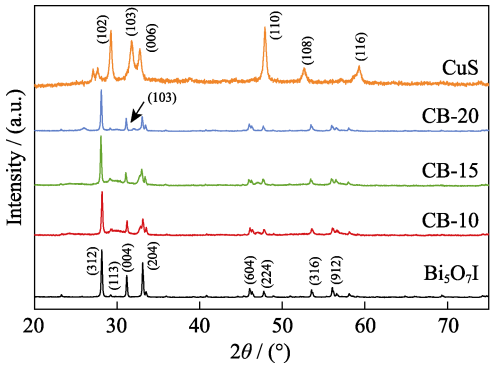

Fig. 1 XRD patterns of Bi_5O_7I, CuS, and CuS/Bi_5O_7I composites

SEM images of the pure Bi_5O_7I and CuS/Bi_5O_7I composites are presented in Fig. 2. It shows that the synthesized Bi_5O_7I exhibits a microrod-like morphology with length of about 3–4 μm and diameters of 200–300 nm. The surface of Bi_5O_7I microrods are smooth which can provide a favorable environment for assembling the co-photocatalyst. After introducing CuS, Bi_5O_7I microrods are covered by thin CuS nanosheets. The CuS nanosheets grow discretely along the axis of Bi_5O_7I microrods. In addition, the nanosheets decorated on Bi_5O_7I microrods become denser with the increasing of CuS mass percentage. Furthermore, the TEM image of CB-15 composite in Fig. 3(a) confirms the SEM results, which illustrates that the surface of Bi_5O_7I microrods is fully and densely covered by irregular shaped CuS nanosheets with strong linkages in the composite. By analyzing the HRTEM images in Fig. 3(b), the lattice spacing of 0.319 nm corresponds to the (312) plane of orthorhombic Bi_5O_7I, and the well crystalline lattice fringe with interplanar spacing of 0.304 nm can be ascribed to (102) plane of CuS, respectively. The interface between the Bi_5O_7I and CuS lattices clearly indicates the formation of CuS/Bi_5O_7I heterojunctions, which is beneficial for the effective separation of photogenerated electron-hole pairs, and thus enhances the photocatalytic activity[20-21].

Chemical states and elemental compositions of CB-15 composite were estimated by XPS spectra. It can be observed in Fig. 4(a), the general survey spectrum reveals

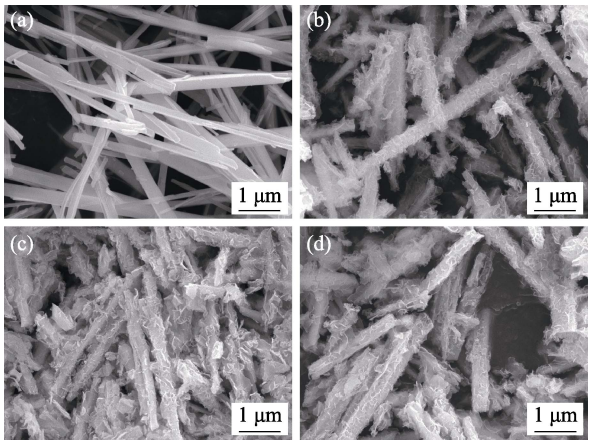

Fig. 2 SEM images of (a) pure Bi_5O_7I, (b) CB-10, (c) CB-15 and (d) CB-20 composites

that the as-prepared CB-15 composite consists of Bi, I, O, Cu and S elements. The signals of C1s located at about 285.3 eV was used for calibration. Fig. 4(b) shows the Bi4f spectrum of CB-15 composite with two peaks at 164.3 and 159.06 eV, which correspond to $Bi4f_{5/2}$ and $Bi4f_{7/2}$, respectively, demonstrating the characteristics of Bi^{3+} ions in the Bi_5O_7I[22]. The high-resolution spectra of I3d show two evident peaks at 618.8 and 630.4 eV (Fig. 4(c)), which can be attributed to $I3d_{5/2}$ and $I3d_{3/2}$, ensuring the monovalent oxidation state of iodine. The O1s spectrum (Fig. 4(d)) was fitted into three peaks centered at 529.6, 531.0 and 532.4 eV, which may be assigned to Bi–O, O–H, and adsorbed H_2O, respectively[23]. In addition, the $Cu2p_{3/2}$ and $Cu2p_{1/2}$ peaks are located at 932.3 and 952.4 eV (Fig. 4(e)), which are characteristic of the Cu^{2+} in the CuS material[24]. As for S2s (Fig. 4(f)), a broad peak at 225.0 eV can be attributed to the metal sulfide[25].

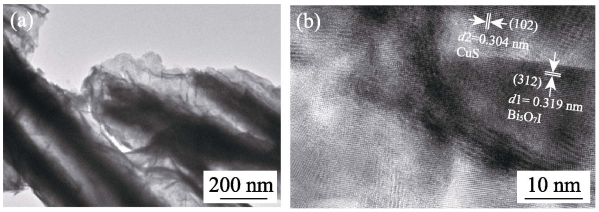

Fig. 3 (a) TEM and (b) HRTEM images of CB-15 composite

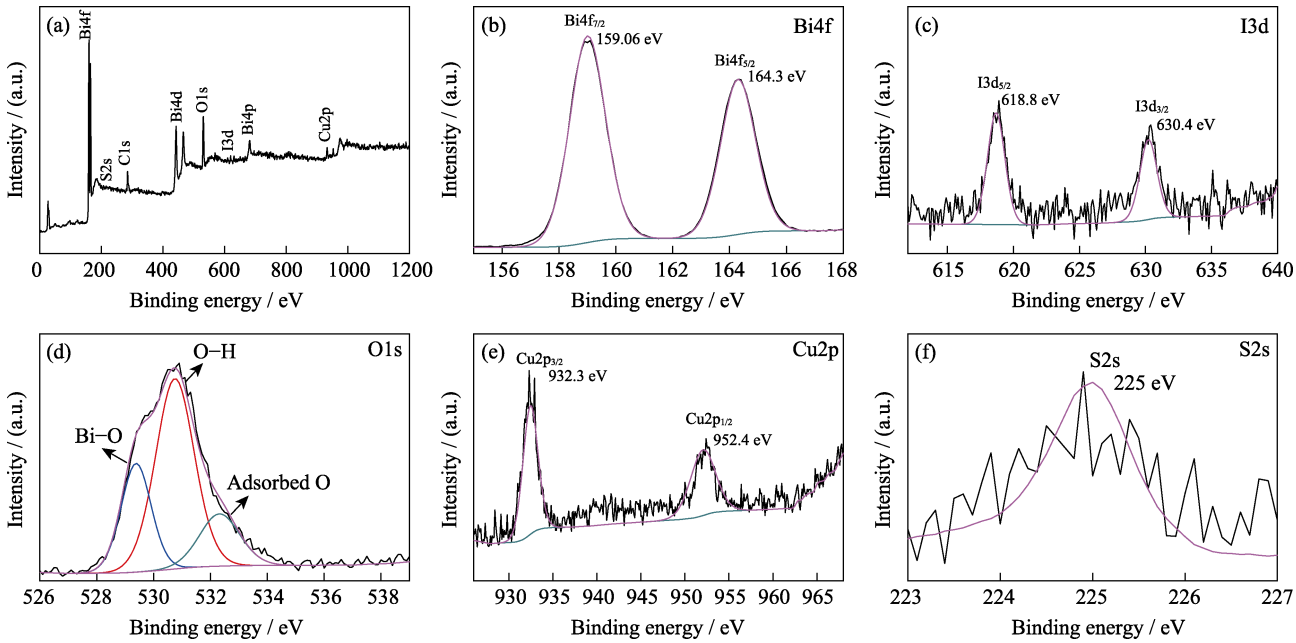

Fig. 4 (a) XPS survey spectrum and high resolution XPS spectra of (b) Bi4f, (c) I3d, (d) O1s, (e) Cu2p, and (f) S2s of CB-15 composite

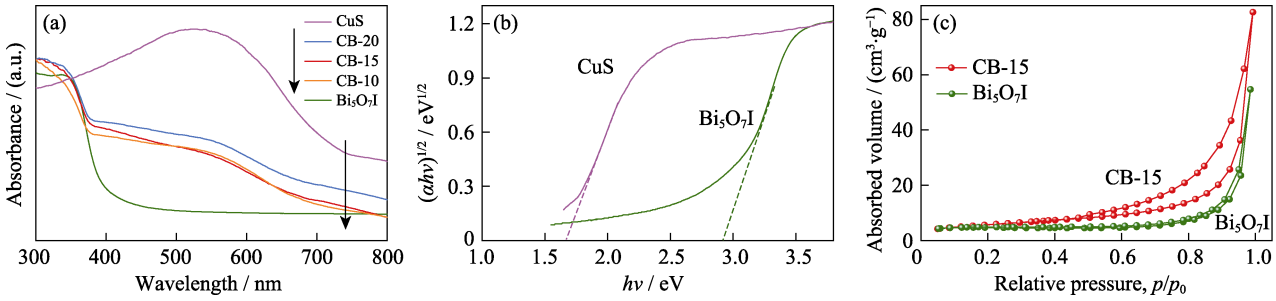

Fig. 5 (a) UV-Vis diffuse reflectance spectra of Bi_5O_7I, CuS and CuS/Bi_5O_7I composites, (b) plots of $(\alpha h\nu)^{1/2}$ *vs* $h\nu$ of Bi_5O_7I and CuS, CuS/Bi_5O_7I composites and (c) N_2 adsorption and desorption isotherms for pure Bi_5O_7I and CB-15 composite

The optical absorption properties of the prepared samples were investigated by UV-Vis diffuse reflectance spectrometer and presented in Fig. 5. Fig. 5(a) indicated that pure Bi_5O_7I microrods has the absorption edge of about 400 nm with a band gap of 2.92 eV calculated based on Kubelka-Munk theory (Fig. 5(b))[17]. The absorption edge of pure CuS is at approximately 740 nm, and the corresponding band gap energy is 1.68 eV. Compared with pure Bi_5O_7I microrods, light absorption of CuS/Bi_5O_7I composites expands to the range of visible light. Moreover, the absorption intensity increased after CuS decorated on Bi_5O_7I microrods. The results of diffuse reflectance spectrometer denote that the decoration of CuS nanosheet on Bi_5O_7I microrods is helpful for the improved visible-light harvesting and photocatalytic activity of CuS/Bi_5O_7I composites[26].

Nitrogen adsorption-desorption isotherms analysis was conducted to investigate the specific surface areas of Bi_5O_7I and CB-15 sample. As shown in Fig. 5(c), the curves of the samples displayed a typical IV feature with a hysteresis loop extended from p/p_0 = 0.5 to p/p_0 = 1 which indicated mesoporous structures of the samples. The BET surface area of CB-15 is 8.77 m^2/g, which is 2.46 times of that of pure Bi_5O_7I (3.56 m^2/g) because the CuS nanosheet decorated Bi_5O_7I microrods have more stretched surfaces compared with Bi_5O_7I microrods. The higher surface area of CB-15 composite is usually closely related to more adsorption sites exposed under irradiation and increased adsorption capability which is, therefore, in favor of the enhanced photocatalytic activity.

Photoluminescence (PL) spectra and electrochemical impedance spectroscopy were further employed to analyze the separation efficiency and recombination rate of photoexcited electrons and holes of Bi_5O_7I and CuS/Bi_5O_7I composites. It can be observed from Fig. 6(a) that the PL spectra of the as-prepared photocatalysts exhibit an obvious emission peak at about 420 nm. The CuS/Bi_5O_7I composites exhibit obviously lower intensity than pure Bi_5O_7I, suggesting that the decoration of CuS nanosheets on Bi_5O_7I microrods can depress the recombination of photogenerated electrons and holes effectively[27]. The faster charge separation would result in increased lifetime of charge carriers and enhanced transfer efficiency of the interfacial charge. Moreover, CB-15 composite shows the lowest intensity, which is consistent with the result of photocatalytic experiment.

Electrochemical impedance spectroscopy (EIS) was conducted to testify the charge migration and recommendation process of the photo-induced carriers in CuS/Bi_5O_7I and at the interface of the composite. The EIS Nyquist plots of Bi_5O_7I and CB-15 composite as illustrated in Fig. 6(b) show that CB-15 composite possesses smaller arc radius. Generally, the smaller radius implies a lower charge transfer resistance[21], which suggests that Bi_5O_7I coupled with a certain amount of CuS is in favor of the separation of photo-generated charge carriers and the interfacial charge transportation[11,28]. Therefore, the EIS results demonstrate that Bi_5O_7I coupled with a certain amount of CuS is in favor of the separation of photo-generated charge carriers and the interfacial charge transportation.

On the basis of the analysis from PL spectra and EIS, the improved photocatalytic reduction of Cr(VI) by the CuS/Bi_5O_7I composite can be attributed to the synergism of the greater surface areas, broader light adsorption and higher separation and transfer efficiency of charge carrier with the CuS decoration on Bi_5O_7I microrods.

Cr(VI) aqueous solutions were used to assess the photocatalytic activity of the CuS/Bi_5O_7I composites, as well as pure Bi_5O_7I and pure CuS. The experiments were carried out under visible light illumination and the results are shown in Fig. 7(a). As can be observed that pure Bi_5O_7I shows low photocatalytic activity with only 12% efficiency after 4 h of visible-light irradiation which can be attributed to the weak absorption in the visible light range. The photoreduction efficiency of Cr(VI) is about 45% in the presence of pure CuS. Under the identical condition, the removal efficiency of Cr(VI) by CuS/Bi_5O_7I was noticeably enhanced, which could be attributed to

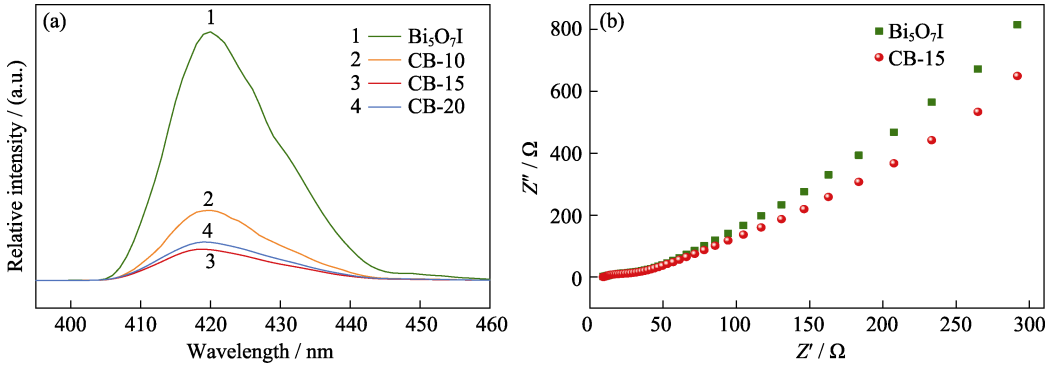

Fig. 6 (a) PL spectra and (b) electrochemical impedance spectra of Bi_5O_7I and CB-15 composite

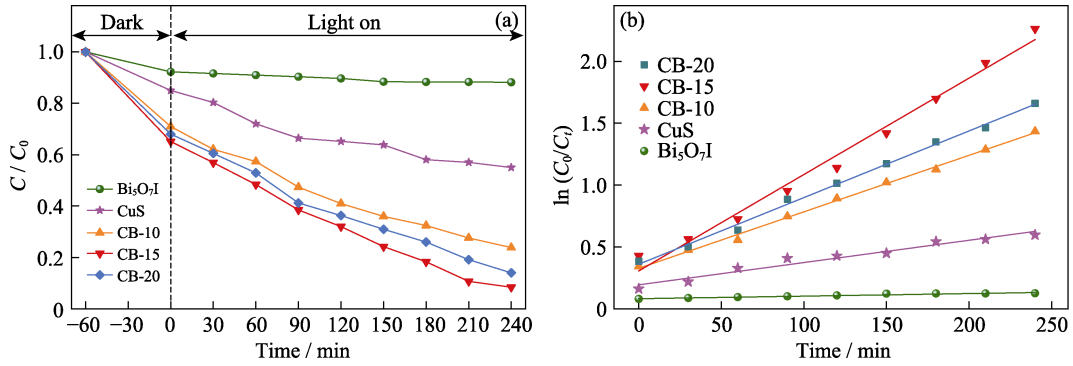

Fig. 7 (a) Photocatalytic efficiency, (b) corresponding kinetic curves for the photocatalytic reduction of aqueous Cr(VI) with Bi_5O_7I and CuS/Bi_5O_7I composites (experimental conditions: 150 mL of 10 mg/L Cr(IV) solution, 100 mg of catalyst)

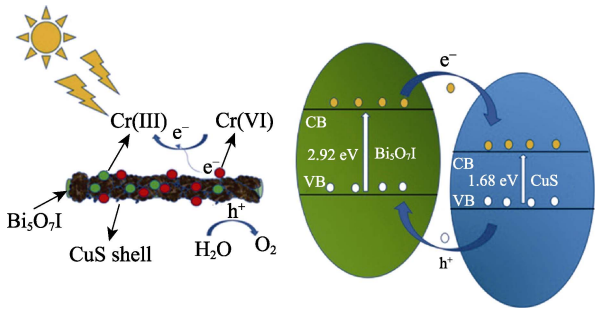

Fig. 8 Schematic diagram of proposed mechanism for photocatalytic reduction of Cr(VI) for CuS/Bi_5O_7I composite under visible light illumination

the higher separation efficiency of photo-excited electrons and holes for the CuS/Bi_5O_7I. On the other hand, it can be obviously found that the photocatalytic activities of CuS/Bi_5O_7I are dependent on CuS content. With the CuS content increasing from 10wt% to 15wt%, the photocatalytic activity reached the maximum with efficiency of about 92%. However, photocatalytic activity decreased with the CuS content further increasing to 20wt%, which indicated that the proper CuS proportion was conducive to the transfer of electrons and holes at interfaces[29]. The photocatalytic reduction kinetic is generally applied to depict the process, and the results are plotted in Fig. 7(b). The photocatalytic reduction process accords to pseudo-first-order kinetics, $\ln(C_0/C_t)=kt$, where C_0 is the initial concentration of the Cr(VI) solution, C_t is the concentration of Cr(VI) at time t, and the slope k is the apparent reaction rate constant. It is apparent than that the apparent reaction rate constants of CuS/Bi_5O_7I composites are greater that of as-prepared Bi_5O_7I. k value of CB-15 is 0.0054 min^{-1}, which confirmed its best photocatalytic performance.

Based on the experimental results and discussion above, the photo-induced electron-hole pairs separation process during the reduction of Cr(VI) by CuS/Bi_5O_7I composite under visible light irradiation was shown in Fig. 8. In general, upon visible illumination, the electrons of Bi_5O_7I and CuS on the valence band (VB) are excited to conduction band (CB), generating holes on the VB which form large number of valence band.

The CB edge potential of Bi_5O_7I is more negative than that of CuS, and the VB position of CuS is positive than that of Bi_5O_7I. As a result, the photoinduced electrons on the Bi_5O_7I nanosheet surface can jump easily to the conduction band of CuS resulting in the reduction of $Cr_2O_7^{2-}$ to Cr^{3+}. By this means, the photo-excited electrons and holes are separated effectively in the CuS/Bi_5O_7I composites and electron-hole recombination behavior is depressed, leading to higher photocatalytic reduction efficiency of Cr(VI) to Cr(III). Consequently, the as-fabricated CuS/Bi_5O_7I composite photocatalyst shows enhanced photocatalytic performance than Bi_5O_7I and CuS.

3 Conclusions

In conclusion, CuS nanosheets decorated Bi_5O_7I composites have been successfully synthesized *via* a facile solution method. CuS/Bi_5O_7I composites exhibit a satisfactory strengthened photocatalytic efficiency for the removal of aqueous Cr(VI) comparing with pure Bi_5O_7I and CuS under visible-light illumination. The photocatalytic reduction rate of Cr(VI) in the presence of CuS/Bi_5O_7I composite with 15wt% CuS is about 20 times of pristine Bi_5O_7I and 3 times of pure CuS. The enhanced photocatalytic activity of CuS/Bi_5O_7I composites is owing to the synergistic effect of the greater surface areas, broader light absorption region, improved charge separation and transfer efficiency of photo-excited electron-hole pairs. This work is helpful for the construction of visible light responsive photocatalytic systems for the practical application involving the treatment of environmental remediation and water purification.

References:

[1] ZHU K R, GAO Y, TAN X, *et al*. Polyaniline modified Mg/Al layered double hydroxide composites and their application in

efficient removal of Cr(VI). *ACS Sustainable Chemistry & Engineering*, 2016, **4:** 4361–4369.

[2] ZHANG S, LI B F, WANG X X, *et al*. Recent developments of two-dimensional graphene-based composites in visible-light photocatalysis for eliminating persistent organic pollutants from wastewater. *Chemical Engineering Journal*, 2020, **390:** 124642.

[3] ZHU K R, CHEN C L, LU S H, *et al*. MOFs-induced encapsulation of ultrafine Ni nanoparticles into 3D N-doped graphene-CNT frameworks as a recyclable catalyst for Cr(VI) reduction with formic acid. *Carbon*, 2019, **148:** 52–63.

[4] HU C Y, LEI E, HU K K, *et al*. Simple synthesis of 3D flower-like g-C_3N_4/TiO_2 composite microspheres for enhanced visible-light photocatalytic activity. *Journal of Materials Science*, 2020, **55(1):** 151–162.

[5] ZHAO G X, SUN Y B, ZHAO Y K, *et al*. Enhanced photocatalytic simultaneous removals of Cr(VI) and bisphenol A over Co(II)-modified TiO_2. *Langmuir*, 2019, **35:** 276–283.

[6] WANG Q L, DONG R F, WANG C, *et al*. Glucose-fueled micromotors with highly efficient visible-light photocatalytic propulsion. *ACS Applied Materials Interfaces*, 2019, **11:** 6201–6207.

[7] CHEN W B, YANG Z F, XIE Z, *et al*. Benzothiadiazole functionalized D-A type covalent organic frameworks for effective photocatalytic reduction of aqueous chromium (VI). *Journal of Materials Chemistry A*, 2019, **7:** 998–1004.

[8] ZHANG R, HAN Q, LI Y, *et al*. Fabrication and characterization of high efficient Z-scheme photocatalyst Bi_2MoO_6/reduced graphene oxide/BiOBr for the degradation of organic dye and antibiotic under visible-light irradiation. *Journal of Materials Science*, 2019, **54:** 14157–14170.

[9] YANG Q, LUO M L, LIU K W, *et al*. A composite of single-crystalline Bi_2WO_6 and polycrystalline BiOCl with a high percentage of exposed (001) facets for highly efficient photocatalytic degradation of organic pollutants. *Chemical Communications*, 2019, **55:** 5728–5731.

[10] SULTANA S, MANSINGH S, PARIDA K. Facile synthesis of CeO_2 nanosheets decorated upon BiOI microplate: a surface oxygen vacancy promoted Z-scheme-based 2D-2D nanocomposite photocatalyst with enhanced photocatalytic activity. *The Journal of Physical Chemistry C*, 2017, **122:** 808–819.

[11] GENG X Q, CHEN S, LÜ X, *et al.* Synthesis of g-C_3N_4/Bi_5O_7I microspheres with enhanced photocatalytic activity under visible light. *Applied Surface Science*, 2018, **462:** 18–28.

[12] WU G J, ZHAO Y, LI Y W, *et al.* Assembled and isolated Bi_5O_7I nanowires with good photocatalytic activities. *CrystEngComm*, 2017, **17:** 2113–2125.

[13] LI B, CHEN X W, ZHANG T Y, *et al.* Photocatalytic selective hydroxylation of phenol to dihydroxybenzene by BiOI/TiO_2 p-n heterojunction photocatalysts for enhanced photocatalytic activity. *Applied Surface Science*, 2018, **439:** 1047–1056.

[14] DONG Z J, PAN J Q, WANG B B, *et al.* The p-n-type Bi_5O_7I-modified porous C_3N_4 nano-heterojunction for enhanced visible light photocatalysis. *Journal of Alloys & Compounds*, 2018, **747:** 788–795.

[15] CHEN Y N, ZHU G Q, GAO J Z, *et al.* Three-dimensional Ag_2O/Bi_5O_7I p-n heterojunction photocatalyst harnessing UV-Vis-NIR broad spectrum for photodegradation of organic pollutants. *Journal of Hazardous Materials*, 2018, **344:** 42–54.

[16] YANG N, X. LÜ X, ZHONG S T, *et al.* Preparation of Z-scheme AgI/Bi_5O_7I plate with high visible light photocatalytic performance by phase transition and morphological transformation of BiOI microspheres at room temperature. *Dalton Transactions*, 2018, **47:** 11420–11428.

[17] MA R, ZHANG S, LI L, *et al.* Enhanced visible-light-induced photoactivity of Type-II CeO_2/g-C_3N_4 nanosheet towards organic pollutants degradation, *ACS Sustainable Chemistry & Engineering*, 2019, **7:** 9699–9708.

[18] KAMRANIFAR M, ALLAHRESANI A, NAGHIZADEH A. Synthesis and characterizations of a novel $CoFe_2O_4$@CuS magnetic nanocomposite and investigation of its efficiency for photocatalytic degradation of penicillin G antibiotic in simulated wastewater. *Journal of Hazardous Materials*, 2019, **366:** 545–555.

[19] LIM W, WU H, LIM Y, *et al.* Facilitating the charge transfer of $ZnMoS_4$/CuS p-n heterojunctions through ZnO intercalation for efficient photocatalytic hydrogen generation. *Journal of Materials Chemistry A*, 2019, **6:** 11416–11423.

[20] DAS K, MAJHI D, BHOI Y, *et al.* Combustion synthesis, characterization and photocatalytic application of CuS/$Bi_4Ti_3O_{12}$ p-n heterojunction materials towards efficient degradation of 2-methyl-4-chlorophenoxyacetic acid herbicide under visible light. *Chemical Engineering Journal,* 2019, **362:** 588–599.

[21] WU R Y, SONG H B, LUO N, *et al.* Microwave-assisted preparation and enhanced photocatalytic activity of Bi_2WO_6/BiOI heterojunction for organic pollutants degradation under visible-light irradiation. *Solid State Science*, 2019, **87:** 101–109.

[22] HU C C, CHEN T S, HUANG H X. Heterojunction of n-type Sr_2TiO_4 with p-type Bi_5O_7I with enhanced photocatalytic activity under irradiation of simulated sunlight. *Applied Surface Science*, 2017, **426:** 536–544.

[23] SUN L X, SUN J H, HAN N, *et al.* rGO decorated W doped $BiVO_4$ novel material for sensing detection of trimethylamine. *Sensors & Actuators B: Chemical*, 2019, **298:** 126749.

[24] LI Q, DU X J, XIA C Q, *et al.* Fabrication and photocatalytic properties of nano CuS/MoS_2 composite catalyst by dealloying amorphous Ti-Cu-Mo alloy. *Applied Surface Science*, 2019, **467–468:** 221–228.

[25] CHAHKANDIA M, ZARGAZI M. Novel method of square wave voltammetry for deposition of Bi_2S_3 thin film: photocatalytic reduction of hexavalent Cr in single and binary mixtures. *Journal of Hazardous Materials*, 2019, **380:** 120879.

[26] CHEN K L, ZHU K R, CHEN K, *et al.* Synthesis of Ag nanoparticles decoration on magnetic carbonized polydopamine nanospheres for effective catalytic reduction of Cr(VI). *Journal of Colloid and Interface Science*, 2018, **526:** 1–8.

[27] ZHANG S, LIU Y, GU P C. Enhanced photodegradation of toxic organic pollutants using dual-oxygen-doped porous g-C_3N_4: mechanism exploration from both experimental and DFT studies. *Applied Catalysis B: Environmental*, 2019, **248:** 1–10.

[28] FEI T, YU L M, LIU Z Y, *et al.* Graphene quantum dots modified flower like Bi_2WO_6 for enhanced photocatalytic nitrogen fixation. *Journal of Colloid and Interface Science*, 2019, **557:** 498–505.

[29] PAN J B, LIU J J, ZUO S L, *et al.* Synthesis of cuboid BiOCl nanosheets coupled with CdS quantum dots by region-selective deposition process with enhanced photocatalytic activity. *Materials Research Bulletin*, 2018, **103:** 216–224.

CuS 纳米片修饰 Bi_5O_7I 复合材料用于光催化还原 Cr(VI)水溶液

蔡 苗, 陈子航, 曾 实, 杜江慧, 熊 娟

(湖北大学 物理与电子科学学院, 铁电压电湖北省重点实验室, 武汉 430062)

摘 要: 光催化技术以其高效、安全、低成本的优势, 被广泛研究用于去除污水中有毒副作用的重金属 Cr(VI)。制备半导体复合材料是一种可以有效提高半导体光催化性能的途径。本研究通过简单的水热法合成了 CuS 纳米片修饰的 Bi_5O_7I 复合材料, 并且表征和评估了其在可见光下对 Cr(VI)的光催化还原活性。与纯 Bi_5O_7I 微米棒及纯 CuS 样品相比, CuS/Bi_5O_7I 复合催化剂对 Cr(VI)水溶液具有更高的光催化降解活性。在相同的可见光辐照条件下, 15wt% CuS 修饰的复合样品, 光催化降解 Cr(VI)的反应常数是纯/Bi_5O_7I 样品的 20 倍, 纯 CuS 样品的 4.3 倍。对比样品的比表面积、光致发光谱和电化学阻抗谱的测试结果发现, 复合样品表现出更高的催化效率是由于 CuS/Bi_5O_7I 具有更大的比表面积、更宽的光吸收区域及更高的光生电子–空穴对的分离和传输效率。本研究还提出了 CuS/Bi_5O_7I 复合材料光催化降解 Cr(VI)的机理。

关 键 词: CuS/Bi_5O_7I 复合光催化剂; 可见光催化剂; 光催化降解 Cr(VI)

中图分类号: O614 **文献标志码**: A